Charge-Driven Transtive Devices via Electric Field Control of Magnetism in a Helimagnet

Yi Sheng Chai[1,2,3] Da Shan Shang,[4] Sae Hwan Chun,[1] Young Sun,[2,3] and Kee Hoon Kim[1,*]

[1]*CeNSCMR and Institute of Applied Physics, Department of Physics and Astronomy, Seoul National University, Seoul 151-747, South Korea*
[2]*Beijing National Laboratory for Condensed Matter Physics, Institute of Physics, Chinese Academy of Sciences, Beijing 100190, China*
[3]*Low Temperature Physics Laboratory, College of Physics, and Center of Quantum Materials and Devices, Chongqing University, Chongqing 401331, China*
[4]*Key Laboratory of Microelectronics Device & Integrated Technology, Institute of Microelectronics, Chinese Academy of Sciences, Beijing 100190, China*

The transtor and memtranstor are the fourth basic linear and memory elements, respectively, which allow direct coupling of charge (q) to magnetic flux (φ) via linear and nonlinear magnetoelectric (ME) effects, respectively. It is found here that a large variation of magnetization by an electric field is realized in both linear and nonlinear hysteretic styles in a magnetoelectric Y-type hexaferrite $Ba_{0.5}Sr_{1.5}Zn_2(Fe_{0.92}Al_{0.08})_{12}O_{22}$ single crystal. Moreover, based on the spin-current model, the underlying microscopic mechanisms for generating the two types of linear and nonlinear M versus E curves are understood to be E-induced changes to the cone angle and sign of P, respectively, establishing the charge-driven transtor and memtranstor in the Y-type hexaferrite system. This work points to a promising pathway to develop alternative circuit functionalities using magnetoelectric materials.

I. INTRODUCTION

In conventional circuit theory, four basic electrical circuit elements, namely, capacitor (C), resistor (R), inductor (L), and memristor, can be defined from the relationship between the four fundamental variables: voltage (v), current (i), charge (q), and magnetic flux (φ) [1–3]. In particular, the memristor is expected to show a nonlinear i-v pinched loop. Inspired by the discovery of the memristor, the memcapacitor and meminductor, which are the nonlinear memory counterparts of the capacitor and inductor, respectively [4], are also proposed based on the observation of pinched q-v and i-φ loops, respectively. Until very recently, contrary to the resistive-switching effects based on the memristor [2], a totally different fourth linear-circuit element, the transtor (T) [5], is proposed to show a direct linear relationship between q and φ [Fig. 1(a)] [5]. Its working mechanism is the so-called magnetoelectric (ME) effect, which refers to the induction of electric polarization (P) by application of a magnetic field (H) (direct ME effect) or, conversely, the induction of magnetization (M) by the application of an electric field (E) (converse ME effect) [6–8]. Similarly, the memtranstor is also expected to exist with a direct nonlinear relationship

between q and φ. With these transtive elements, a unified and complete picture of the relational diagram for the fundamental circuit elements can be established. In other words, a complete circuit diagram is expected to demonstrate four linear-circuit elements, R, C, L, and T, and four nonlinear elements, memristor (M_R), memcapacitor (M_C), meminductor (M_L), and memtranstor (M_T). [See Fig. 1(a) for a pictorial representation [5].]

The ME-based transtive device can then be composed of a block of ME materials sandwiched between two parallel electrodes to operate in either a longitudinal ($E \| M$ or $H \| P$) or a transverse ($E \perp M$ or $H \perp P$) configuration [5], as shown in the inset of Fig. 2(b). Such a device in the transverse configuration can be proved theoretically to exhibit a direct link between φ passing through the flank side and q induced on the electrodes by

$$q = DS = (\varepsilon_0 E + P)S = \varepsilon_0 \varepsilon_r ES + \alpha HS, \quad (1)$$

where $D = \varepsilon_0 E + P$ is the electric displacement and α is the ME coefficient. The magnetic flux, φ, passing through the flank side would be

$$\varphi = BS' = \mu_0(H + M)S' = \alpha ES' + \mu_0 \mu_r HS', \quad (2)$$

where $B = \mu_0(H + M)$ represents the magnetic induction. Here, S and S' are the areas of ME media beneath the

---

*khkim@phya.snu.ac.kr
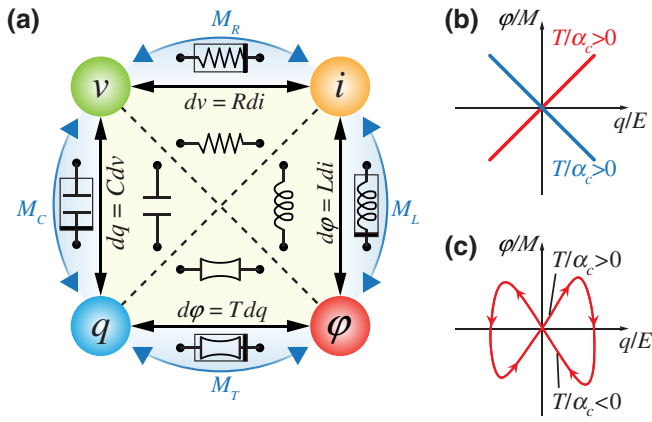
(a)

(b)

(c)

FIG. 1.   (a) Complete relational diagram of all possible fundamental two-terminal circuit elements, both linear and nonlinear, which correlate a particular pair of the four basic circuit variables, i.e., charge q, voltage v, current i, and magnetic flux φ. Nonlinear memory devices corresponding to the four linear fundamental elements, i.e., resistor (R), capacitor (C), inductor (L), and transtor (T), are accordingly termed as memristor (M_R), memcapacitor (M_C), meminductor (M_L), and memtranstor (M_T). (b) Schematic illustration of charge-driven transtive behavior, which is anticipated to directly correlate φ with q with positive or negative T values (or, equivalently, a linear change of M under E with either positive or negative α_C in ME materials). (c) Characteristic behavior of the charge-driven memtranstor, showing a butterfly hysteresis loop between q and φ. Butterfly-shaped loop in (c) occurs at sufficiently large input of q (or, equivalently, a butterfly shape of M under E in ME materials with a large enough E to induce a sign change in α_C).

electrodes and the flank side, respectively. ε_0 is the vacuum permittivity, ε_r is the relative permittivity of the medium, μ_0 is the permeability of vacuum, and μ_r is the relative permeability of the medium. From Eqs. (1) and (2), we can deduce that

$$d\varphi = \frac{S'}{S} \frac{\alpha_C}{\varepsilon_0 \varepsilon_r} dq, \tag{3}$$

for a charge-driven transtive device based on the converse ME effect, or

$$dq = \frac{S}{S'} \frac{\alpha_D}{\mu_0 \mu_r} d\varphi, \tag{4}$$

for a flux-driven transtive device based on the direct ME effect. $\alpha_D = dP/dH$ and $\alpha_C = \mu_0 dM/dE$ are the direct and converse ME coefficients, respectively (they usually have similar values with the same sign). In both cases, the transtance quantity, $T = d\varphi/dq$, can be defined to characterize the performance of the ME transtive device. Notably, T can be either positive or negative, depending on the sign of α_C [see Fig. 1(b) for the converse ME effect]. On the other hand, the memtranstor requires a butterfly-shaped hysteresis in the φ-q loop that corresponds to the hysteresis

in the M-E or P-H loop [only the q-driven case is shown in Fig. 1(c)].

With these linear and nonlinear ME effects, transtive devices have already shown great application potential as nonvolatile multilevel random-access memory [9–12], complete Boolean logic gates [13], and a synaptic-plasticity-based neural network model [14,15]. In particular, a charge-driven transtive element employing the converse ME effect would be more practical for electric circuits. For example, nonvolatile memory based on the nonlinear converse ME effect, termed transtance-change random-access memory (TCRAM), is proposed [12]. The electrical writing of the TCRAM requires a butterfly-shaped hysteresis M-E loop in the ME medium to tune the signs and values of α_C and T electrically [Fig. 1(c)]. The realization of a charge-driven memtranstor would open a way to realize next-generation intelligent devices with circuit functionality. Although the charge-driven devices are realized only with ME composite structures [9–12], to miniaturize them further, a single-phase ME material would be more favorable. The control of M by E is a difficult task in single-phase materials, while the realization of a butterfly-shaped hysteresis of the M-E loop [Fig. 1(c)] is even more challenging. Therefore, the demonstration of a charge-driven memtranstor in single-phase materials is yet to be realized.

The Y-type hexaferrite $Ba_{0.5}Sr_{1.5}Zn_2(Fe_{0.92}Al_{0.08})_{12}O_{22}$ consists of a series of Fe/Zn-O tetrahedral and Fe/Al-O octahedral layers stacked along the [001] direction [16]. Under an in-plane magnetic field cooling or a high-magnetic-field history, this compound exhibits a commensurate transverse conical ordering based on a previous neutron-diffraction study [17], as shown in Fig. 2(a), in which the alternating small (S) and large (L) magnetic blocks have antiparallel in-plane components with a modulation vector of $k_0 = (0,0,3/2)$. From the spin-current (or inverse Dzyaloshinskii-Moriya) mechanism [18,19], ferroelectric polarization can be induced by the transverse cone, where $P \propto \sum_{ij} k_0 \times (S_i \times S_j)$, and S_i and S_j are spins on the two adjacent sites along the [001] direction. The induced P will be always perpendicular to H and k_0, as shown in Fig. 2(a). In the transverse-cone phase of $Ba_{0.5}Sr_{1.5}Zn_2(Fe_{0.92}Al_{0.08})_{12}O_{22}$, a giant ME coefficient, $\alpha_D \sim 2 \times 10^4$ pm/s, is found at zero H at 30 K [20]. Conversely, an E control of large-M reversal at zero H is also realized in $Ba_{0.5}Sr_{1.5}Zn_2(Fe_{0.92}Al_{0.08})_{12}O_{22}$ below 170 K due to its large α_C [21]. Therefore, it is a good candidate material to realize the functionalities of a charge-driven transtor and memtranstor.

Here, we investigate E control of M under large-bias dc magnetic fields in an ME Y-type hexaferrite $Ba_{0.5}Sr_{1.5}Zn_2(Fe_{0.92}Al_{0.08})_{12}O_{22}$ single crystal. By varying the strength of H bias, both linear and nonlinear converse ME effects are selectively controlled. Our findings reveal that $Ba_{0.5}Sr_{1.5}Zn_2(Fe_{0.92}Al_{0.08})_{12}O_{22}$ can
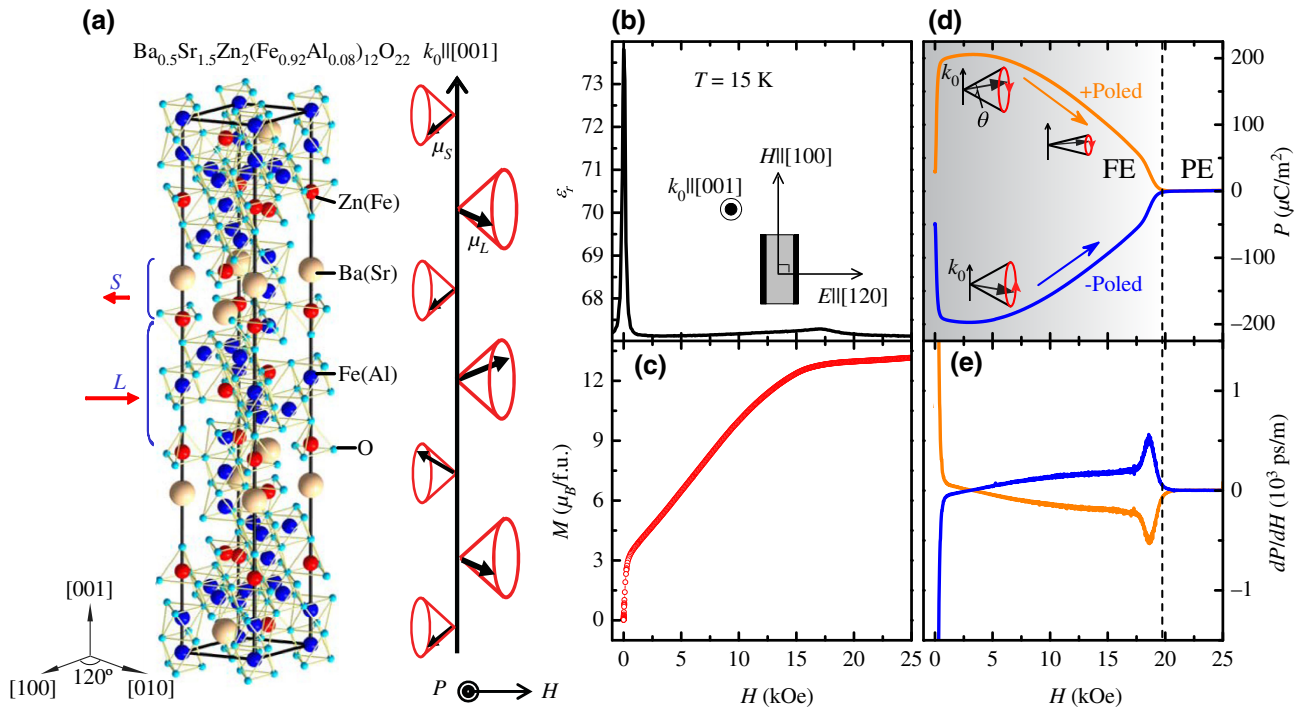
FIG. 2. (a) Schematic illustration of the crystal and transverse-cone magnetic structure of $Ba_{0.5}Sr_{1.5}Zn_2(Fe_{0.92}Al_{0.08})_{12}O_{22}$. Transverse-cone spin configuration propagates along a commensurate modulation vector, $k_0 = (0,0,3/2)$; μ_L and μ_S denote net magnetic moments in magnetic L and S blocks, respectively. According to the spin-current mechanism, ferroelectricity (FE) and an in-plane P perpendicular to both H and k_0 can be induced. Magnetic field dependence of (b) relative dielectric constant ε_r, (c) magnetization M, (d) polarization P, and (e) dP/dH of $Ba_{0.5}Sr_{1.5}Zn_2(Fe_{0.92}Al_{0.08})_{12}O_{22}$ at 15 K after magnetic field cooling processes. Measurement configuration is illustrated in the inset of (b). In the inset of (d), the cone opening angle, θ, is expected to be suppressed with increasing H between 3 and 19 kOe. Sign of P is directly correlated to spin-rotation directions. Above 19 kOe, spin configuration becomes collinear, that is, it is paraelectric (PE).

serve as an ME medium for a charge-driven transtor and memtranstor based on the linear and butterfly-shaped φ-q relationships, respectively.

II. METHODS

The Y-type hexaferrite $Ba_{0.5}Sr_{1.5}Zn_2(Fe_{0.92}Al_{0.08})_{12}O_{22}$ single crystals are grown from a Na_2O-Fe_2O_3 flux in air and annealed at 900°C in a flow of oxygen to enhance the resistivity [20]. The starting chemicals are mixed with a molar ratio of $BaCO_3$:$SrCO_3$:ZnO:Fe_2O_3:Al_2O_3:Na_2O = 2.95:16.74:19.69:49.32:4.29:7.01. A single crystal is cut into a rectangular shape for electric measurements along the [120] direction, while H is along the [100] direction, so that $E \perp H \perp k_0$, as shown in the inset of Fig. 2(b). Towards this end, the temperature and magnetic field are supplied by a physical property measurement system (PPMS, Quantum Design, USA). In a magnetoelectric poling procedure, the magnetic field is applied along the [100] direction, and the electric field is applied along the [120] direction of the sample. To achieve magnetoelectric poling conditions of either +poled or −poled status, an electric field of $E = 220$ kV m^{-1} is applied to the sample at 120 K, while the magnetic field is varied from 20 to 12 kOe to bring

the crystal from the paraelectric and collinear phase to the ferroelectric and transverse-cone phase. Then the sample is cooled to 15 K. Finally, the electric field is first turned off, and then the magnetic field is ramped to the required value for the forthcoming electric measurements. The magneto-electric current is measured and integrated to determine the change in electric polarization with magnetic field by a high-resistance electrometer (Keithley 6517B). The same procedure is adopted for measurements under −poled conditions, with the direction of electric field reversed. Magnetization curves are measured using a vibrating sample magnetometer in a PPMS (Quantum Design). For magnetization measurements under a biased electric field, the sample temperature is maintained at 15 K. For magnetization measurements under an electric field, the sample holder of the conventional vibrating sample magnetometer is modified to tolerate a high electric field.

III. RESULTS AND DISCUSSION

A. Magnetic and direct ME properties of $Ba_{0.5}Sr_{1.5}Zn_2(Fe_{0.92}Al_{0.08})_{12}O_{22}$

To reveal the ferroelectricity of $Ba_{0.5}Sr_{1.5}Zn_2(Fe_{0.92}Al_{0.08})_{12}O_{22}$, the target temperature is chosen to be 15 K,

where $Ba_{0.5}Sr_{1.5}Zn_2(Fe_{0.92}Al_{0.08})_{12}O_{22}$ is reported to show H-induced ferroelectricity and strong ME coupling below 20 kOe [20]. At 15 K, H-dependent electric and magnetic measurements are performed, as shown in Figs. 2(b) and 2(e). In Fig. 2(b), the H-dependent relative dielectric constant, ε_r, exhibits two clear peaks at around 0 and 19 kOe, respectively, where a transverse cone and ferroelectric phase is expected to exist between the fields. Accordingly, the H-dependent M curve also shows two kinks at similar H values, as seen in Fig. 2(c). As H increases, the M-H curve shows a rapid increase from 0 to about 0.5 kOe, a less-sharp increase from 0.5 to 19 kOe, and then the curve is almost saturated above 20 kOe. Above 19 kOe, $Ba_{0.5}Sr_{1.5}Zn_2(Fe_{0.92}Al_{0.08})_{12}O_{22}$ enters the ferrimagnetic phase [17]. The existence of ferroelectricity between 0 and 19 kOe is confirmed with nonzero P by integrating the ME currents as a function of time [Fig. 2(d)] as well as the sign reversal of P by the reversed poling of E in this field region. The sign of P in a transverse-cone state is then determined by the sign of spin helicity, $\sum_{ij} S_i \times S_j$, that is, the sign is determined by whether the spins in the transverse-cone phase rotate in clockwise or counterclockwise directions, as shown in the inset of Fig. 2(c). Above 19 kOe, the ferrimagnetic phase is PE because $S_i \times S_j = 0$ for collinear spins.

Moreover, there is a strong H dependence in the P behavior in the FE phase. The absolute P value ($|P|$) shows a rapid increase below 0.5 kOe and reaches a plateau between 0.5 and 3 kOe [Fig. 2(d)]. However, a further increase of H decreases $|P|$ gradually and finally makes it zero above 19 kOe, where $Ba_{0.5}Sr_{1.5}Zn_2(Fe_{0.92}Al_{0.08})_{12}O_{22}$ is paraelectric. Accordingly, a huge nonzero dP/dH ($=\alpha_D$) can be calculated, as shown in Fig. 2(e). For the $+P$ case, α_D shows a giant positive peak centered at zero H (not fully shown here), which quickly approaches zero above 0.5 kOe, monotonically decreases, and becomes negative between 0.5 and 18 kOe before vanishing above 19 kOe. The large α_D within the FE phase should have magnetic origins. The zero-field peak in α_D comes from the in-plane rotation of the transverse-cone domains between ± 3 kOe [21]. However, the sign reversal of the α_D value between 3 and 19 kOe must have a different physical origin. One can easily expect that, with increasing H, the transverse-cone opening angle, θ, will decrease accordingly [inset of Fig. 2(d)], thus decreasing the P values induced by the spin-current mechanism. It can naturally explain the simultaneously increase of M and decrease of P in the field range of 3–19 kOe. Finally, the peaks near 18 kOe in the dP/dH curves indicate the onset H of the transition from the transverse cone to the collinear ferrimagnetic phases.
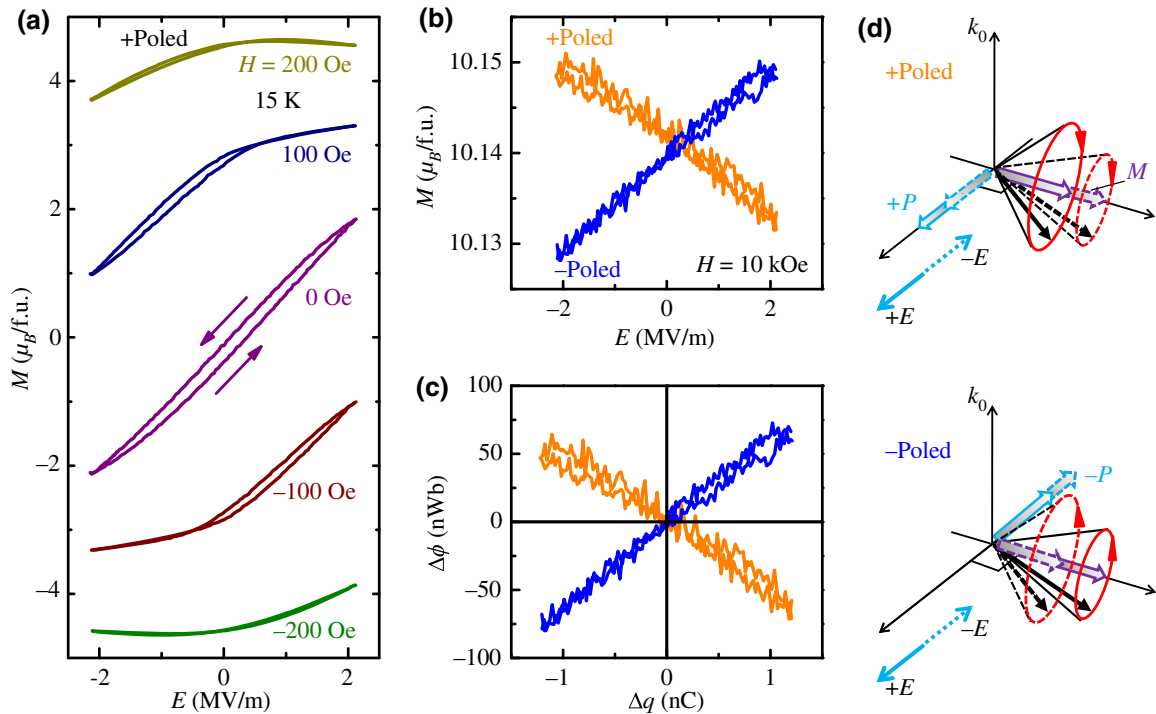

FIG. 3. (a) Electric field (E) dependence of M under different low-dc magnetic fields (H) at 15 K. Clear hysteresis behavior can be seen in M-E loops for $H = 100, 0,$ and -100 Oe. Strong quadratic ME behavior is clear for $H = \pm 200$ Oe. Data at $H = 0$ Oe are from Ref. [14]. (b) Nearly linear ME behavior for both +poled and −poled cases under $H = 10$ kOe. (c) Converted ϕ-q relationship [from (b)] of the transtor made from $Ba_{0.5}Sr_{1.5}Zn_2(Fe_{0.92}Al_{0.08})_{12}O_{22}$. (d) Schematic diagrams of the change in the cone opening angle under external E for +poled (upper panel) and −poled (lower panel) cases. Solid and dashed lines represent P and M of the cone under $+E$ and $-E$, respectively.

Following Eq. (2), the nonzero α_D observed in $Ba_{0.5}Sr_{1.5}Zn_2(Fe_{0.92}Al_{0.08})_{12}O_{22}$ means that a flux-driven transtor, with a device configuration as shown in the inset of Fig. 2(b) and using the crystal as the working medium, can be actualized and operated in the parameter domain specified above. The different signs of α_D for +poled and −poled cases result in different signs of transtance T. As we mention above, it is more challenging to realize charge-driven transtive devices, since the demonstration of E control of M is much harder and rarer than that of H control of P. However, we have already demonstrated in $Ba_{0.5}Sr_{1.5}Zn_2(Fe_{0.92}Al_{0.08})_{12}O_{22}$ a giant dM/dE, i.e., the converse ME effect at zero H [21]. The converse ME effect at zero H shows a small hysteresis [Fig. 3(a)], making it not ideal for either a transtor or a memtranstor [5]. By applying a small-dc biased magnetic field, the hysteresis behavior of the M-E loops is suppressed, while the linear ME behavior is replaced by quadratic ME behavior [Fig. 3(a)], which is also unfavorable for the transtive devices. In the following, we will show that, by applying a stronger-dc H bias, we can still realize nearly ideal charge-driven transtor and memtranstor devices based on $Ba_{0.5}Sr_{1.5}Zn_2(Fe_{0.92}Al_{0.08})_{12}O_{22}$.

B. Linear converse ME effect and charge-driven transtor of $Ba_{0.5}Sr_{1.5}Zn_2(Fe_{0.92}Al_{0.08})_{12}O_{22}$

We first apply a constant bias of $H = 10$ kOe to drive the system to the single-magnetic transverse-cone-domain state with a finite α_D. A slowly varying E is found to induce a nearly linear M response, yielding nonzero α_C ($=\mu_0 dM/dE$ in this case), as shown in Fig. 3(b). α_C also allows both positive and negative values, depending on the poling condition, while, for the same poling condition, α_C and α_D share the same sign. No hysteresis or a very-small quadratic component is shown in such curves. To understand the underlying physics, the effects of E on M can be considered as an inverse process of H over P. As schematically illustrated in Fig. 3(d), the electric field can change the magnitude of polarization and indirectly causes a change in the transverse-cone opening angle, θ, or, in other words, a change in magnetization. Depending on the different initial ME poling condition, E can enhance or reduce M, resulting in the opposite sign of α_C, which is consistent with our observations.

With the help of the above scenario, the M-E curves for $Ba_{0.5}Sr_{1.5}Zn_2(Fe_{0.92}Al_{0.08})_{12}O_{22}$ can be readily converted into $\Delta\varphi$-Δq response curves in the device made of $Ba_{0.5}Sr_{1.5}Zn_2(Fe_{0.92}Al_{0.08})_{12}O_{22}$, as shown in Fig. 3(c). For data in Fig. 3(b) with dc $H = 10$ kOe, we can easily find that $\Delta q_{ME} = \varepsilon_0 \varepsilon_r \Delta ES$ from Eq. (1). From Eq. (2), $\Delta\phi = \mu_0(\Delta H + \Delta M)S' = \mu_0 \Delta M S'$. Its transtance ($T = \Delta\varphi/\Delta q$) is either positive or negative, depending on the poling condition. The above $\Delta\varphi$-Δq relationship perfectly fits to a

typical charge-driven transtor. Therefore, such a mechanism makes other ME hexaferrites with a transverse-cone state good candidates for the charge-driven transtors.

C. Nonlinear converse ME effect and charge-driven memtranstor of $Ba_{0.5}Sr_{1.5}Zn_2(Fe_{0.92}Al_{0.08})_{12}O_{22}$

Additionally, the same device turns out to be a charge-driven memtranstor when the biased dc H is set to be 18 kOe, where $|dP/dH|$ shows a peak feature. This H value can drive the $Ba_{0.5}Sr_{1.5}Zn_2(Fe_{0.92}Al_{0.08})_{12}O_{22}$ crystal to approach the FE-PE phase boundary. In this case, the magnetic response becomes double-periodically tuned to the driving E after the first 12.5 s, and it is always nonlinear [Fig. 4(a)]. By redrawing the time-varying data for E and M in Fig. 4(a) to the M-E curves in Fig. 4(b), a butterfly-shaped loop can be clearly identified, with the crossing point of the curves for upward and downward sweeps of E in the vicinity of $E = 0$. Such a butterfly-shaped M-E loop under constant H corresponds to a butterfly-shaped $\Delta\varphi$-Δq loop in Fig. 4(d) for the model device, where $\Delta q = (\varepsilon_0 \Delta E + P)S = \varepsilon_0 \varepsilon_r \Delta ES$ and $\Delta\phi = \mu_0(\Delta H + \Delta M)S' = \mu_0 \Delta M S'$. The opposite slopes for the $\Delta\varphi$-Δq curves in the region from point 1 to point 2 and that from point 3 to point 4 refer to the opposite signs of transtance, T, values. Therefore, our device with the $Ba_{0.5}Sr_{1.5}Zn_2(Fe_{0.92}Al_{0.08})_{12}O_{22}$ crystal indeed demonstrates characteristic behavior of a charge-driven memtranstor.

To understand further the physical process involved in the butterfly-shaped M-E loop, we carefully check data in Fig. 4(b). From point 1 to point 2, $\alpha_C < 0$ indicates positive P in this region, as illustrated in the upper panel of Fig. 3(d). From point 2 to point 3, α_C suddenly becomes positive, indicating negative P, i.e., the polarization is reversed by a negative electric field. In the region between point 3 and point 4, $\alpha_C > 0$ again, confirming that negative P is maintained during the process. Finally, from point 4 to point 5, α_C suddenly becomes negative, indicating positive P, i.e., the polarization is reversed again by a positive electric field. The above processes are schematically demonstrated in Fig. 4(c). In the meantime, P reversal implies a reverse of the spin helicity due to the spin-current mechanism in the ferroelectricity. In other multiferroics with spiral or conical ordering, e.g., $TbMnO_3$ and $MnWO_4$, the reversal of spin helicity upon the reversal of P has already been reported in neutron-diffraction studies [22,23]. It is very likely that there will be a hysteresis of polarization following slow E sweeping near the FE-PE phase boundary. Usually, for ferroelectrics, the coercive field is zero at the phase boundary, and it becomes larger as it moves away from the boundary. In the Y-type hexaferrite we study, the FE phase resides between ± 19 kOe at 15 K, so the high magnetic field is closer to the boundary, while the low magnetic field is away from the boundary. Therefore, the butterfly curve appears at high magnetic field with low ME
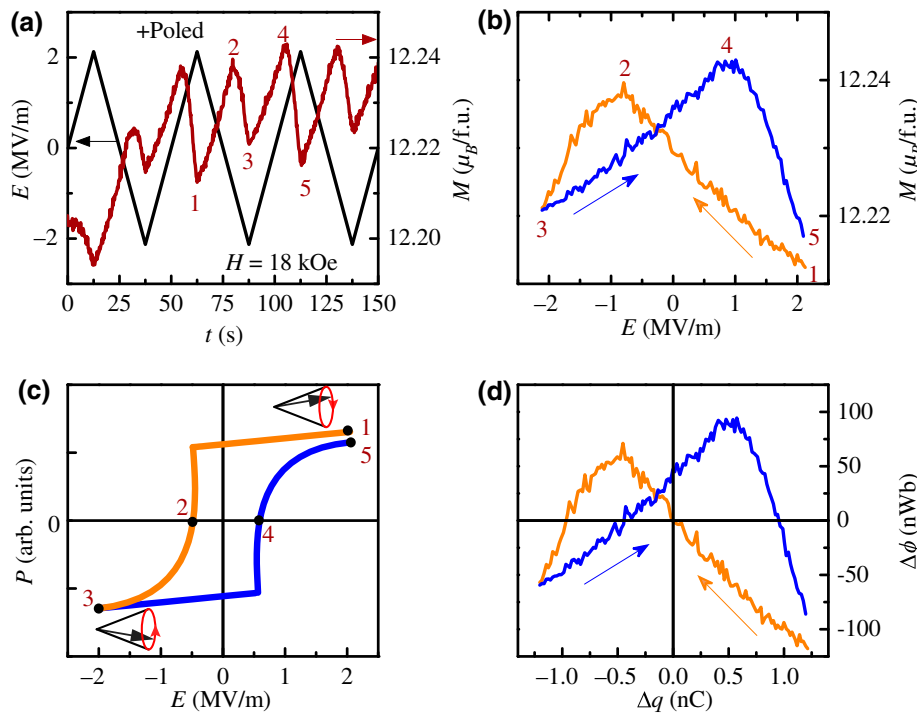
FIG. 4. (a) Nonlinear modulations of magnetization, M, at 18 kOe and 15 K by repeating triangular waves of E after +poled. From points 1 to 5, E is swept from 2.1 to -2.1 MV/m and back to 2.1 MV/m again. (b) Butterfly-shaped M-E loop, illustrating data in (a), spanning the range from points 1 to 5. (c) Schematic diagram of the P-E loop from points 1 to 5. Notably, point 1 and point 3 should have different cone-rotation directions. Accordingly, their signs of P and α_C are opposite. (d) Butterfly-shaped M-E loop in (b) can be directly converted into a memtranstive φ-q loop.

coupling, but not at low fields with high ME coupling. In our case, the E values at points 2 and 4 represent negative and positive coercive E, respectively [Fig. 4(c)].

In this material, the boundary between FE and PE persists up to at least 220 K [20], where the butterfly-shaped M-E loop is allowed. However, due to the leakage nature of this sample at high temperature, we cannot utilize a high enough E to observe this hysteresis behavior. The above underlying physics demonstrates the memtranstive principle, which can be readily applicable to other single-phase ME systems with a heliconical spin ordering. There are plenty of magnetoelectric hexaferrites that show heliconical spin configurations under a magnetic field, and many of these can retain this order around room temperature, or even higher, with substantial ME coupling [24]. Moreover, in the domain-reversal processes, the relaxation mechanism will play a role, since more domains with opposite P will be reversed for a longer time. The timescale of the spin-reversal process can be very fast, which points to a much shorter device *on-off* period.

It is worth pointing out that the memtransistor demonstrated in $Ba_{0.5}Sr_{1.5}Zn_2(Fe_{0.92}Al_{0.08})_{12}O_{22}$ does not have an ideal butterfly-shaped loop, i.e., it is not pinched at $E = 0$, due to the existence of tiny spontaneous polarization. From Eq. (1), spontaneous polarization will supply a nonzero initial value of q, leading to a crossing of the hysteretic loop that is slightly shifted from zero E. Even with the deviation from a zero-driving field for the hysteresis loops, the behavior exhibited by our model device using the converse ME effect, or specifically the differential relationships between φ and q, still meets the definition for

the fourth fundamental memelement in an extended sense. Similar behavior is observed in other memristive devices, so memristive, memcapacitive, and meminductive systems can be extended to dynamic cases where pinching occurs elsewhere from the zero-driving field [25].

IV. CONCLUSIONS

Electric field control of large magnetization changes are realized in both linear and butterfly-shaped hysteresis patterns with two underlying mechanisms in magnetoelectric Y-type hexaferrite $Ba_{0.5}Sr_{1.5}Zn_2(Fe_{0.92}Al_{0.08})_{12}O_{22}$ single crystal at 15 K. Based on this magnetoelectric material system, the expected fourth circuit elements, a charge-driven transtor and memtranstor with linear and nonlinear relationships between φ and input q, respectively, are unambiguously demonstrated via the achieved converse magnetoelectric behavior. The two mechanisms of E control of M will be very helpful for developing more circuit functionalities with ME hexaferrites in the future.

[1] L. O. Chua, Memristor-The missing circuit element, IEEE Trans. Circuit Theory **18**, 507 (1971).

[2] D. B. Strukov, G. S. Snider, D. R. Stewart, and R. S. Williams, The missing memristor found, Nature **453**, 80 (2008).

[3] L. O. Chua and S. M. Kang, Memristive devices and systems, Proc. IEEE **64**, 209 (1976).

[4] M. D. Ventra and Y. V. Pershin, Circuit elements with memory: Memristors, memcapacitors, and meminductors, Proc. IEEE. **97**, 1717 (2009).

[5] D. S. Shang, Y. S. Chai, Z. X. Cao, J. Lu, and Y. Sun, Toward the complete relational graph of fundamental circuit elements, Chin. Phys. B **24**, 068402 (2015).

[6] H. Schmid, Introduction to the proceedings of the 2nd international conference on magnetoelectric interaction phenomena in crystals, Ferroelectrics **161**, 1 (1994).

[7] J.-P. Rivera, On definitions, units, measurements, tensor forms of the linear magnetoelectric effect and on a new dynamic method applied to Cr-Cl boracite, Ferroelectrics **161**, 165 (1994).

[8] W. Brown Jr, R. Hornreich, and S. Shtrikman, Upper bound on the magnetoelectric susceptibility, Phys. Rev. **168**, 574 (1968).

[9] J. X. Shen, J. Z. Cong, Y. S. Chai, D. S. Shang, S. P. Shen, K. Zhai, Y. Tian, and Y. Sun, Nonvolatile Memory Based on Nonlinear Magnetoelectric Effects, Phys. Rev. Appl. **6**, 021001 (2016).

[10] J. X. Shen, D. S. Shang, Y. S. Chai, Y. Wang, J. Z. Cong, S. P. Shen, L. Q. Yan, W. H. Wang, and Y. Sun, Nonvolatile Multilevel Memory and Boolean Logic Gates Based on a Single $Ni/[Pb(Mg_{1/3}Nb_{2/3})O_3]_{0.7}[PbTiO_3]_{0.3}/Ni$ Heterostructure, Phys. Rev. Appl. **6**, 064028 (2016).

[11] J. X. Shen, J. Z. Cong, D. S. Shang, Y. S. Chai, S. P. Shen, K. Zhai, and Y. Sun, A multilevel nonvolatile magnetoelectric memory, Sci. Rep. **6**, 34473 (2016).

[12] P. P. Lu, D. S. Shang, J. X. Shen, Y. S. Chai, C. S. Yang, K. Zhai, J. Z. Cong, S. P. Shen, and Y. Sun, Nonvolatile transtance change random access memory based on magnetoelectric P (VDF-TrFE) / metglas heterostructures, Appl. Phys. Lett. **109**, 252902 (2016).

[13] J. Shen, P. Lu, D. Shang, and Y. Sun, Realization of Complete Boolean Logic Functions Using a Single Memtranstor, Phys. Rev. Appl. **12**, 054062 (2019).

[14] P. Lu, J. Shen, D. Shang, and Y. Sun, Artificial synaptic device based on a multiferroic heterostructure, J. Phy. D: Appl. Phys. **52**, 465303 (2019).

[15] J. X. Shen, D. S. Shang, Y. S. Chai, S. G. Wang, B. G. Shen, and Y. Sun, Mimicking synaptic plasticity and neural network using memtranstors, Adv. Mater. **30**, 1706717 (2018).

[16] J. Smit and H. P. J. Wijn, *Ferrites* (Philips Technical Library, Eindhoven, 1959), pp. 278.

[17] H. B. Lee, Y.-S. Song, J.-H. Chung, S. H. Chun, Y. S. Chai, K. H. Kim, M. Reehuis, K. Prokeš, and S. Mat'aš, Field-induced incommensurate-to-commensurate phase transition in the magnetoelectric hexaferrite $Ba_{0.5}Sr_{1.5}Zn_2(Fe_{1-x}Al_x)_{12}O_{22}$, Phys. Rev. B **83**, 144425 (2011).

[18] H. Katsura, N. Nagaosa, and A. V. Balatsky, Spin Current and Magnetoelectric Effect in Noncollinear Magnets, Phys. Rev. Lett. **95**, 057205 (2005).

[19] M. Mostovoy, Ferroelectricity in Spiral Magnets, Phys. Rev. Lett. **96**, 067601 (2006).

[20] S. H. Chun, Y. S. Chai, Y. S. Oh, D. J. Nagar, S. Y. Haam, I. G. Kim, B. S. Lee, D. H. Nam, K.-T. Ko, J.-H. Park, J.-H. Chung, and K. H. Kim, Realization of Giant Magnetoelectricity in Helimagnets, Phys. Rev. Lett. **104**, 037204 (2010).

[21] Y. S. Chai, S. Kwon, S. H. Chun, I. Kim, B. G. Jeon, K. H. Kim, and S. Lee, Electrical control of large magnetization reversal in a helimagnet, Nat. Commun. **5**, 4208 (2014).

[22] Y. Yamasaki, H. Sagayama, T. Goto, M. Matsuura, K. Hirota, T. Arima, and Y. Tokura, Electric Control of Spin Helicity in a Magnetic Ferroelectric, Phys. Rev. Lett. **98**, 147204 (2007).

[23] A. Arkenbout, T. Palstra, T. Siegrist, and T. Kimura, Ferroelectricity in the cycloidal spiral magnetic phase of $MnWO_4$, Phys. Rev. B **74**, 184431 (2006).

[24] T. Kimura, Magnetoelectric hexaferrites, Annu. Rev. Condens. Matter Phys. **3**, 7 (2012).

[25] I. Valov, E. Linn, S. Tappertzhofen, S. Schmelzer, J. Van Den Hurk, F. Lentz, and R. Waser, Nanobatteries in redox-based resistive switches require extension of memristor theory, Nat. Commun. **4**, 1771 (2013).